IEEE Access
Multidisciplinary | Rapid Review | Open Access Journal

Received September 11, 2019, accepted September 25, 2019, date of publication October 1, 2019,
date of current version October 11, 2019.

Digital Object Identifier 10.1109/ACCESS.2019.2944840

A Piezoelectric Stick-Slip Nanopositioning Stage With Ultra-High Load Capacity Realizing by Decoupling the Driving and Moving Units

YANG YU[1], QIANG GAO[1], XIAOSONG ZHANG[1], GUANGDA QIAO[1], YI HAN[2], XIAOHUI LU[1], AND TINGHAI CHENG[1,3]

[1]School of Mechatronic Engineering, Changchun University of Technology, Changchun 130012, China
[2]School of Mechanical Engineering, The University of Melbourne, Melbourne, VIC 3010, Australia
[3]Beijing Institute of Nanoenergy and Nanosystems, Chinese Academy of Sciences, Beijing 100083, China

Corresponding author: Tinghai Cheng (chengtinghai@163.com)

This work was supported in part by the Technology Research Planning Project of Education Department of Jilin Province under Grant JJKH20181037KJ and Grant JJKH20191293KJ, in part by the Project of Industrial Technology Research and Development of Jilin Province Development and Reform Commission under Grant 2019C037-6, and in part by the Science and Technology Development Plan of Jilin Province under Grant 20190201108JC.

ABSTRACT The stick-slip piezoelectric stage plays an important role in micro-operation and industrial applications due to its nanometer resolution. However, under high load, the output performance of the piezoelectric stage will be seriously influenced. In order to overcome this limitation, this paper proposes a piezoelectric stick-slip nanopositioning stage with ultra-high load capacity by introducing the load unit to decouple the driving and moving units. A kinetic model of prototype is established to analyze the working process. And a series of experiments are carried out to explore the output performance of the prototype. The geometry of the prototype is 85 mm (*Length*)×50 mm (*Width*)×32 mm (*Height*), and the mass of it is 303 g. By using only one piezoelectric stack, this prototype can achieve load capacity more than 10 kg and driving capacity more than 47.62 [(mm/s)g/mW] in both directions. When there is free-load, under the sawtooth waveform of 100 V at 600 Hz, the velocity of the prototype can reach 4.75 mm/s and 4.86 mm/s in forward and backward directions respectively. Meanwhile, the forward and backward resolution of the prototype can attain 30 nm and 33 nm, respectively. When the load is 10 kg which is about 33 times larger than the weight of prototype, the velocity of the prototype is almost the same as the velocity under free-load.

INDEX TERMS Stick-slip, nanopositioning stage, ultra-high load capacity, high resolution.

I. INTRODUCTION

High-precision stage with nanometer resolution plays a vital part in precision drive and manipulation, such as ultra-precision machining [1], [2], nanometer measurement [3], [4], and biomedical [5]. With the development of precision positioning technology, there are other requirements for high-precision stages, such as long travel range, high resolution, high velocity, large driving force or load capacity [6], [7]. The traditional positioning mechanisms, such as ball screws and sliding rails, can hardly satisfy the continuous requirements. Therefore, some new driving methods and principles are developed [8], [9].

The associate editor coordinating the review of this manuscript and approving it for publication was Zheng Chen.

Piezoelectric materials act an extremely essential in high-precision positioning owing to their small size, high resolution and rapid response [10], [11]. Consequently, piezoelectric stages are widely used in the above fields [12], [13]. According to the operating principle, they can mainly be divided into four types, which are direct driving type [14], [15], ultrasonic type [16]–[20], inchworm type [21] and stick-slip type [22]–[24]. Piezoelectric stages of the direct driving type can achieve high resolution, large force, and reliable output performance [25]. Nevertheless, the motion stroke has only several micrometers. Ultrasonic type piezoelectric stages are powered by high driving voltage and frequency which is resonance frequency [26], [27]. They can also obtain high velocity and compact size, but the wear and the heat generation are still problems. The motion principle

of the inchworm-type piezoelectric stages is a type of bionic which imitates the movement of the inchworm in nature [28]. They can achieve large force and high resolution. But they always need at least three phases, so they have complex structures. The piezoelectric stages of stick-slip type are powered by friction force and usually composed by a driving unit and a moving unit (usually a slider) [29]. The motion stroke of stick-slip type piezoelectric stages is just limited by the length of moving unit. They can also achieve high resolution and high motion velocity. However, their output performance will be influenced greatly due to the change of inertial force and friction force under high load, which affects the application area of stick-slip type piezoelectric stages. So, some studies have been proposed by researchers to improve the load capacity of piezoelectric stages.

Xie *et al*. use a form-closed cam to separate the driving unit and moving unit, and the study reduces the influence of step displacement when the load is increased [30]. Rong *et al*. use various force couple driving and a rotor to overcome the effect of high load on positioning accuracy [31]. In addition, in our previous work, we proposed a composite waveform [32], [33]. The composite wave is realized by applying high-frequency since wave to the rapid deformation phase of the sawtooth wave to reduce the friction force in the ''slip'' phase and improve the load capacity of actuator. The studies have greatly improved the load capacity of the stick-slip type piezoelectric stages. However, owing to the varied friction force between the driving unit and moving unit, if the loads are unbalanced or under the high load, the output performance will be influenced seriously.

Therefore, a piezoelectric stick-slip nanopositioning stage with ultra-high load capacity by introducing the load unit to decouple the driving and moving units is proposed. At the same time, the output performance (velocity, effective displacement) can achieve a good linear relationship with the various driving voltages and frequencies in forward and backward directions. Section I describes the research background of piezoelectric stages and the novelty of this work. Section II shows the structure and the motion principle of the prototype. Section III presents the kinetic models of common piezoelectric stage and prototype, and the working process is analyzed. Section IV shows that a series of experiments are tested to explore the output performance of prototype. At last, section V concludes this paper.

II. STRUCTURE AND MOTION PRINCIPLE

A. STRUCTURE DESIGN

The three dimensional model of the piezoelectric stick-slip nanopositioning stage is shown in Fig. 1(a). The stage mainly consists of four parts: driving unit, moving unit, load unit and a base. The driving unit consists of a piezoelectric stack and a frictional rod. The moving unit consists of springs, adjusting bolts and preload blocks. In addition, the load unit consists of a load board and sliders. As shown in Fig. 1(b), the driving unit and moving unit are connected with the two preload

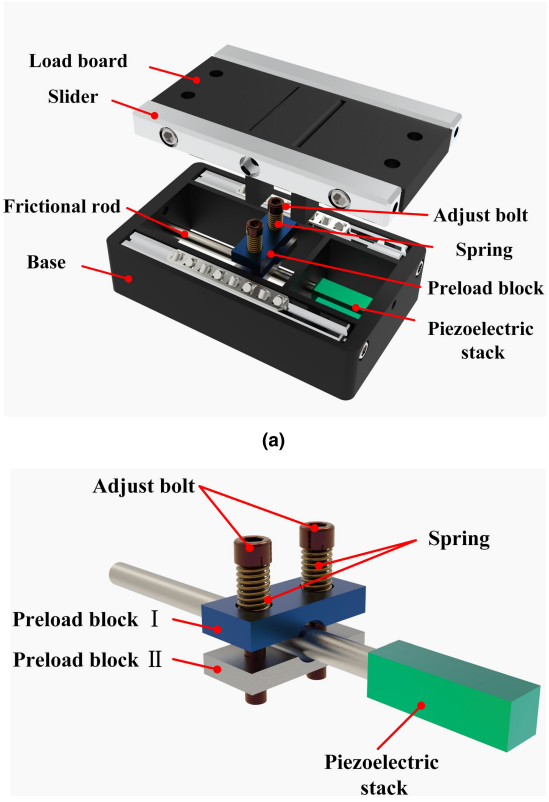

FIGURE 1. The three dimensional model: (a) The piezoelectric stick-slip nanopositioning stage; (b) The driving unit and the moving unit.

blocks through the two adjust bolts. These two adjust bolts connect with preload block I and preload II. Due to the friction force between the preload blocks and the frictional rod, the preload blocks can move when a voltage signal excites the piezoelectric. The friction force is only influenced by the compression of spring. When a load on the stage, it will be undertaken by the load unit, and will not influence the friction force between driving unit and moving unit. Furthermore, the designed piezoelectric stick-slip nanopositioning stage can achieve ultra-high load capacity.

B. MOTION PRINCIPLE

The operation principles of the common stage and proposed stage are compared and shown in Fig. 2. A sawtooth waveform voltage (slow increase and rapid decrease) is chosen to drive the piezoelectric stack. When the two stages under free-load, they will have the same status. The motion principle can be described as three steps:

In initial phase: at time t_0, piezoelectric stack is at natural length.

In stick phase: from t_0 to t_1, with the driving voltage increasing, the moving unit has the same displacement as the piezoelectric stack extends a length d_1 due to the static friction force between the moving unit and driving unit.

In slip phase: from t_1 to t_2, the piezoelectric stack recovers the natural length with the voltage decreasing rapidly.

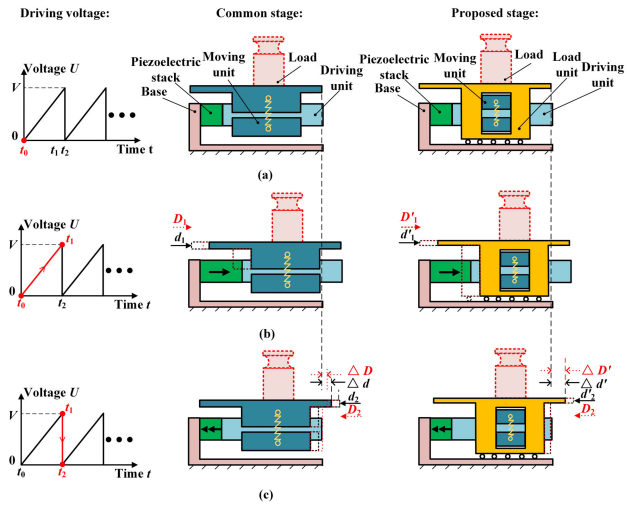

FIGURE 2. Operation principle: (a) Initial phase. (b) Stick phase. (c) Slip phase.

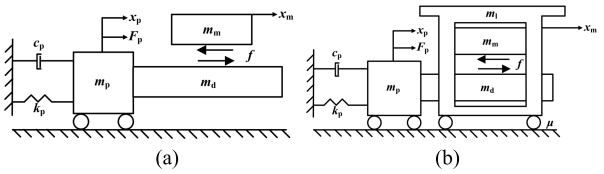

FIGURE 3. Kinetic model of stage: (a) Common stage. (b) Proposed stage.

The moving unit has a reverse displacement d_2 due to the dynamic friction force between the moving unit and driving unit.

Therefore, the displacement of the piezoelectric stage is $\Delta d(\Delta d = d_1 - d_2)$. By repeating the above steps, the moving unit can achieve a long motion in the forward direction. It can also move a long motion in the backward direction by changing the input sawtooth waveform voltage (rapid increase and slow decrease). The piezoelectric stages can also achieve stick-slip, stick-stick, slip-stick and slip-slip motion process with the different driving frequency [34].

When the two stages with varied loads, the motion principle is described. For the common stage, the displacement of the stage will decrease because the friction force between the driving unit and moving unit increases. As the load continues to increase, the displacement ΔD (ΔD is the displacement of the prototype under the load) gradually approaches zero [24]. But the stage proposed in this paper can overcome this limitation. When a load is added, the movement trend of proposed stage is almost the same as that under free-load $\left(\Delta D' \approx \Delta d'\right)$. This is because the added load doesn't affect the friction force between the driving unit and the moving unit.

III. KINETIC MODELING AND ANALYSIS

As shown in Fig. 3, there are two kinetic models established to explain the working process.

No matter the piezoelectric stack extends or curtails, there may exist two situations: stick phase and slip phase. It depends on the maximum friction force between the driving and moving units F_s. If the acceleration of the piezoelectric stack $\left|\ddot{x}_p\right|$ is equal or less than the maximum acceleration of the moving unit (the ratio of F_s to m_m), it is stick phase, otherwise it is slip phase. The kinetic function of the common stage can be described as follows (the movement direction of the prototype is positive):

In stick phase (when $\left|\ddot{x}_p\right| \leqslant \left|\frac{F_s}{m_m}\right|$):

$$F_p = \left(m_p + m_d + m_m\right)\ddot{x}_p + c_p\dot{x}_p + k_p x_p \left(x_p = x_m\right) \quad (1)$$

In slip phase (when $\left|\ddot{x}_p\right| > \left|\frac{F_s}{m_m}\right|$):

$$F_p = \left(m_p + m_d\right)\ddot{x}_p + c_p\dot{x}_p + k_p x_p + m_m\ddot{x}_m \left(x_p \neq x_m\right) \quad (2)$$

where m_p, c_p, k_p, x_p and F_p represent the mass, damping coefficient, stiffness, the osutput displacement and the output force of the piezoelectric stack, respectively. m_d and m_m represent the mass of the driving unit and moving unit. x_m is the displacement of the moving unit. According to the analysis, there are four motion situations for the piezoelectric stage: stick-slip (the stage can move in forward direction), stick-stick (the stage can't move), slip-stick (the stage can move in backward direction), slip-slip (the stage can move fast). Therefore, the slip is the necessary condition to make the stage move.

So, relatively large $|\ddot{x}_p|$ and small F_s are beneficial to the movement of the stage. The $|\ddot{x}_p|$ is influenced by the driving voltage, driving frequency and the size of piezoelectric stack. F_s is influenced by the preload force and the load. For the common piezoelectric stage, with the load increasing, the output performance will decline due to the increasing of F_s. But the output performance of piezoelectric stage proposed by this paper is seldom influenced by the high load.

Based on the cross-roller linear guides, a new structure is proposed by decoupling the driving and moving units. The kinetic model of the proposed stage is shown in Fig. 3 (b). Because the friction coefficient μ between the base and load unit is the cross-roller linear guides which is very small, the load unit can be ignored.

When there is a load on the stage: the horizontal force of the load unit is shown in Fig. 4. The load unit sustains two forces in horizontal direction. One of them is the driving force f which is the friction force between the driving unit and moving unit. The other is friction force F_d.

$$F_d = \mu\left(m_1 + m_w\right)g \quad (3)$$

It is a negative force, and it is influenced by the load and friction coefficient μ. If $f \geqslant F_d$, the stage can move stably. Otherwise, the stage can't move. The maximum of f is F_s, and the mass m_w of the load can be calculated as follows:

$$F_s \geqslant F_d \quad (4)$$

Then

$$F_s \geqslant \mu\left(m_1 + m_w\right)g \quad (5)$$

That is

$$m_w \leqslant \frac{F_s}{\mu g} - m_1 \quad (6)$$

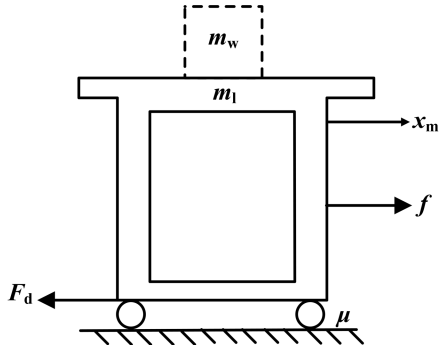

FIGURE 4. The horizontal force of the load unit.

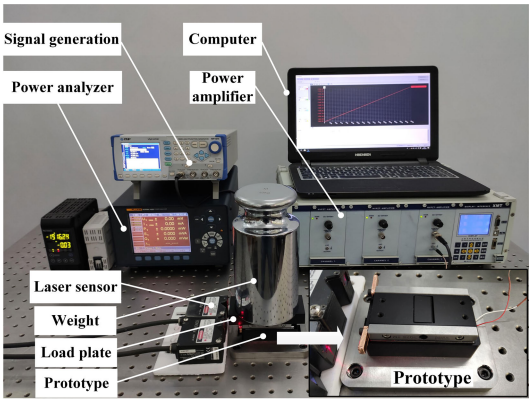

FIGURE 5. The established experimental system and prototype.

Because in this prototype, μ is quite small, the m_w can be very large. Thus, the proposed stage obtains the ultra-high load capacity.

IV. EXPERIMENTS

In this section, a prototype is proposed and the experimental system is established. A series of experiments are tested to explore the output performance of prototype.

A. PROTOTYPE AND EXPERIMENT SETUP

The prototype and the established experimental system are shown in Fig. 5. The geometry of the prototype is 85 mm×50 mm×32 mm. For the prototype, AE0505D16F (NEC/TOKIN) with a size of 5 mm (L)×5 mm (W)×20 mm (H) is chosen as the power source. Two cross-roller linear guides from THK are selected, because of their small friction coefficient and large load capacity. AL7075 is selected as the material of the base and load board. The material of the frictional rod is carbon fiber. The experimental system mainly consists of a power analyzer, an arbitrary signal generator, a power amplifier, two laser sensors, a prototype, a computer and a series of weights (1 kg, 2 kg, 3 kg, 4 kg, 5 kg and 10 kg). The sawtooth waveform voltage signals are supplied by the arbitrary signal generator (WF1974, Negative Feedback Corporation). The sawtooth waveform voltage signals are amplified by the power amplifier (XE-500-C, Harbin Core Tomorrow Science and Technology Corporation) to drive the prototype and the input power can be measured by the power

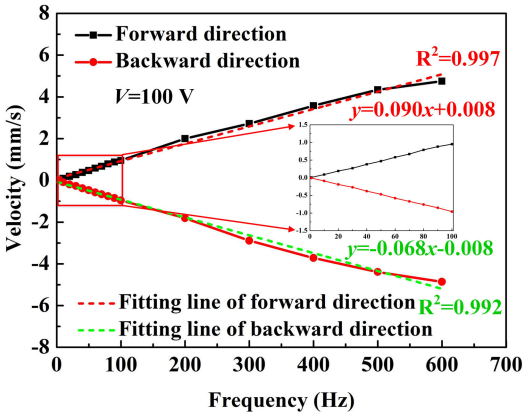

FIGURE 6. Relationship between the driving frequency and output velocity.

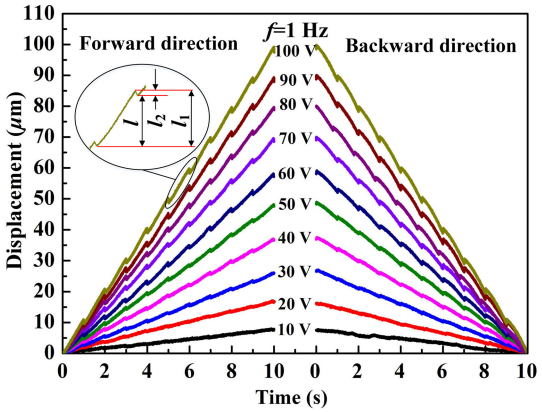

FIGURE 7. Displacement under various driving voltage.

analyzer (NORMA4000, FLUKE Corporation). By using two laser sensors (LK-H020, Keyence Corporation) with the resolution of 20 nm, the velocity and the displacement of the prototype are measured simultaneously. Additionally, a series of weights are used to test the performance of the stage under different loads.

B. EXPERIMENTAL RESULTS

First of all, the frequency characteristic is investigated when the driving voltage is 100 V. The velocities of the prototype in both directions are tested under various driving frequencies. As shown in Fig. 6, the velocity in forward direction is almost the same as the velocity in backward direction under the same driving frequency. In addition, the relevant fitting lines are solved. And the correlation coefficients are 0.997 and 0.992, which shows the velocity of the prototype increases linearly with the frequency increasing. When the driving frequency is 600 Hz, the velocity of the prototype can reach 4.75 mm/s and 4.86 mm/s in forward and backward directions, respectively.

As the magnified shows in Fig. 6, the velocity of the prototype has the better linear relationship with lower driving frequency which is benefit to control. So, the prototype is suitable for working at lower driving frequency. Fig. 7 shows the displacements of the stage in both directions under different driving voltages from 10 V to 100 V in steps of 10 V with

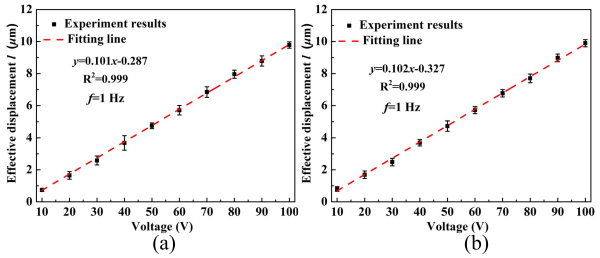

FIGURE 8. The effective displacement of the stage with various driving voltages: (a) in forward direction. (b) in backward direction.

a constant frequency of 1 Hz. The accumulated displacement of the 10 steps by the prototype in forward direction is almost the same as that in backward direction. Additionally, the displacements of the stage increase linearly with the increasing of driving voltage. So, the appropriate driving voltage can be selected to satisfy the required displacements. Furthermore, the effective displacement l can be calculated as follows:

$$l = l_1 - l_2 \tag{7}$$

where l_1 is the displacement of the stage during stick phase. l_2 is the displacement of the stage during slip phase. And the ratio of backward motion η which is a very important parameter of piezoelectric stage can be described as follows:

$$\eta = \frac{l_2}{l} \times 100\% \tag{8}$$

Now, $\eta > 0$, if we want to make $\eta = 0$, we can improve the driving voltage and the driving frequency [34], decrease the preload force [24] or adopt the special institution design.

The effective displacement l of the stage is measured in different directions under various driving voltages with a constant driving frequency of 1 Hz. The average value of the 10 steps is calculated as the real effective displacement under the particular voltage. The effective displacements in both directions are shown in Fig. 8(a) and Fig. 8(b) respectively. It can be seen that the effective displacements and driving voltage are a positive correlation in both directions. The maximum of effective displacements in forward and backward directions are 9.78 μm and 9.89 μm. At the same time, the relevant fitting curve has been solved in both directions, respectively. The correlation coefficients are both $R^2 = 0.999$, which shows the effective displacement has a good linear relationship with the driving voltage. The reason is due to the compact structure and the output displacement is transferred by the piezoelectric stack directly, instead of using mechanisms. Therefore, the proposed of the prototype reduces the error sources in the motion process.

The resolution of the prototype is measured with the frequency of 1 Hz in Fig. 9. A driving voltage of 4.8 V is selected in which the stage can move stably in both directions. The experiment results have a little fluctuation due to the air vibration and environmental noise. And the Fast Fourier Transform (FFT) is selected to filter the experiment results. Finally, the resolution of the stage in both directions are

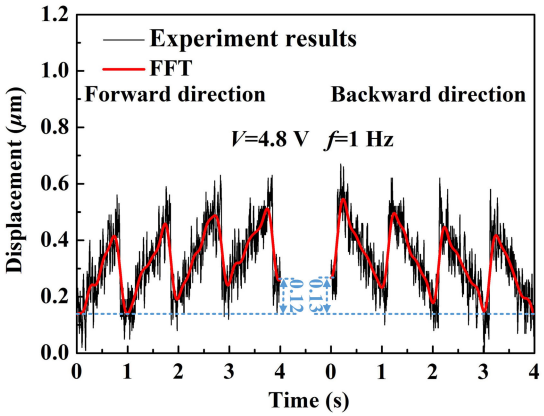

FIGURE 9. The resolution of the stage.

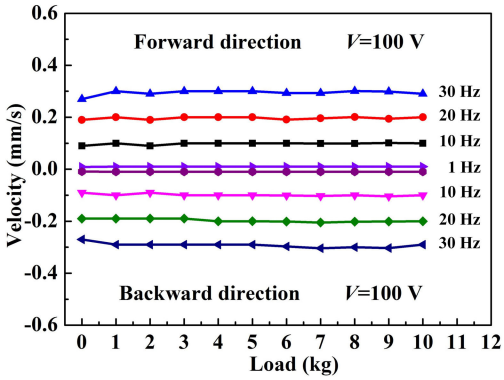

FIGURE 10. The relationship between velocity and load.

measured which are 30 nm and 33 nm in forward and backward directions, respectively.

The load capacity of the piezoelectric stages is a very important parameter which influences their application area. So, the load capacity of the prototype is investigated. Fig. 10 shows the relationship between velocity and load with a constant driving voltage of 100 V in both directions. The experiment results show that when the driving frequency is 1 Hz, 10 Hz, 20 Hz and 30 Hz, the forward velocity and the backward velocity of the prototype almost keep constant with the high load. In addition, we can predict the load capacity of the prototype is more than 10 kg which is almost 33 times greater than the mass of prototype (303 g).

Fig. 11 shows the displacement of the prototype in forward direction with the driving frequency of 1 Hz, 10 Hz, 20 Hz and 30 Hz, under the load of 0kg and 10 kg when the driving voltage is 100 V. It can be seen that the prototype can move stably even though the load is 10 kg. During the 1-second time of motion, the accumulated displacement errors under different driving frequency are listed in table 1. At the same driving frequency, the displacement of the prototype under the load of 10 kg is a little greater than that under the load of 0 kg. This is because the prototype under the load of 10 kg will have larger inertia force. In addition, the ratio of backward motion η of prototype under the load of 0 kg and 10 kg is shown in table 1. And the ratio of backward motion η decreases with the driving frequency increases. When the load is 10 kg

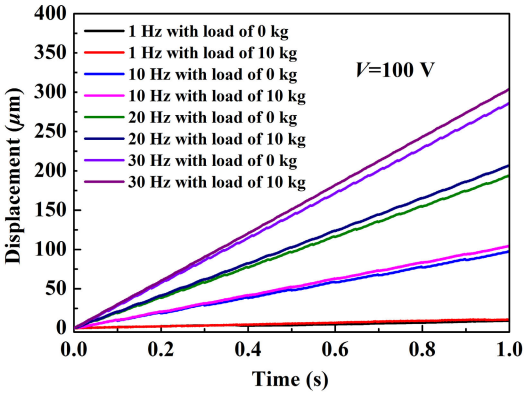

FIGURE 11. The displacement of the prototype with different driving frequency under load of 0 kg and 10 kg.

TABLE 1. The displacement performance of the prototype.

Driving frequency(Hz)	1	10	20	30
Displacement error during the 1-second time(μm)	1.50	7.65	13.16	18.00
Ratio of backward motion with the load of 0 kg (%)	9.05	8.42	7.68	6.39
Ratio of backward motion with the load of 10 kg (%)	8.28	5.92	~0.00	~0.00

and the driving frequency is 20 Hz, the ratio of backward motion η is close to 0. The reason of $\eta > 0$ is that the velocity of the prototype is negative value at time t_2 as shown in Fig. 2. If the driving frequency increases, the velocity of the prototype will increase at time t_1, so it will increase the velocity of the prototype at time t_2. When the velocity of the prototype is 0 mm/s at time t_2, the ratio of the backward motion is just 0. And with the driving frequency continuing to increase, the principle of the prototype will change from stick-slip to slip-slip [34].

In order to illustrate the output performance of the prototype, a new parameter, driving capacity C_d is defined as follows [33], [35]:

$$C_d = \frac{m_w \times v}{P_i} \tag{9}$$

where m_w is the mass of the load. v is the velocity of the prototype under different loads. P_i is the input power, which can be measured by power analyzer (NORMA4000, FLUKE Corporation) directly.

The output performance of the prototype is almost same in both directions. Therefore, the driving capacity C_d of the prototype in forward direction is calculated and discussed. The experimental results are shown in Fig. 12. For the same driving frequency, the driving capacity C_d increases linearly with the increasing load. This is because the input power is influenced by driving voltage and driving frequency, when driving voltage and frequency are fixed, as well as the input power. Moreover, the velocity of prototype v is almost the same with varied loads. For the different driving frequency, with the same load, the driving capacity C_d is almost constant. The reason is that the velocity v and the input power P_i have a linear relationship with the driving frequency for the prototype. So the ratio of v to P_i is almost constant.

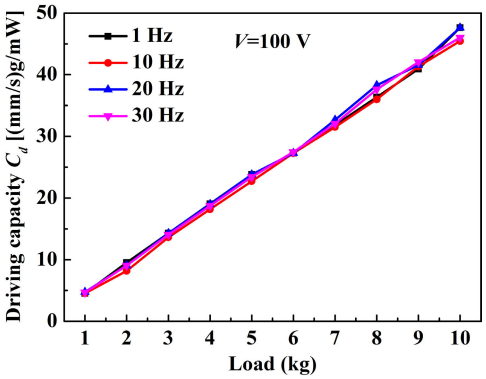

FIGURE 12. The relationship between driving capacity C_d and load.

TABLE 2. The proposed stage compares with literature stages.

Stick-slip stages with a large load capacity	Input driving voltage (V)	Free-load Velocity (mm/s)	Load capacity (kg)
Xie [30]	100	—	>0.15
Cheng [33]	100	0.410	0.36
Li [36]	100	0.742	3.60
Zhao [37]	100	0.088	1.00
Prototype	100	~4.800	>10.00

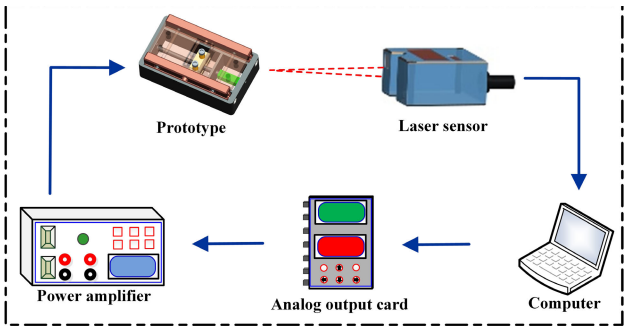

FIGURE 13. The schematic of experimental process.

The maximum of driving capacity C_d is 47.62 [(mm/s)g/mW] in the curve which is more than 10 times as the driving capacity in previous work [33]. Because the load capacity of stage is more than 10 kg, we can predict the maximum of driving capacity C_d of the prototype surpasses 47.62 [(mm/s)g/mW].

The main performance of the stick-slip stages is listed in table 2 to compare with the performance of the prototype. Obviously, the proposed stick-slip piezoelectric stage, even with the same input driving voltage, can achieve the load capacity over 10 kg, which is the best of others. At the same time, the proposed stick-slip piezoelectric stage has good performance in velocity.

At last the macro-micro positioning method is used to explore the positioning resolution of the proposed stage. And the schematic of experimental process is shown in Fig. 13. The laser sensor is used to test the displacement of the prototype, and the test results will be recorded by the computer.

In the experiment, the test results are collected as the feedback signal by Labview and control the output signal of the analog output card by MATLAB. The detail control process

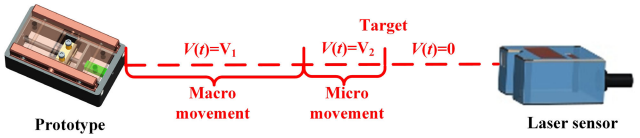

FIGURE 14. The detail control of the prototype.

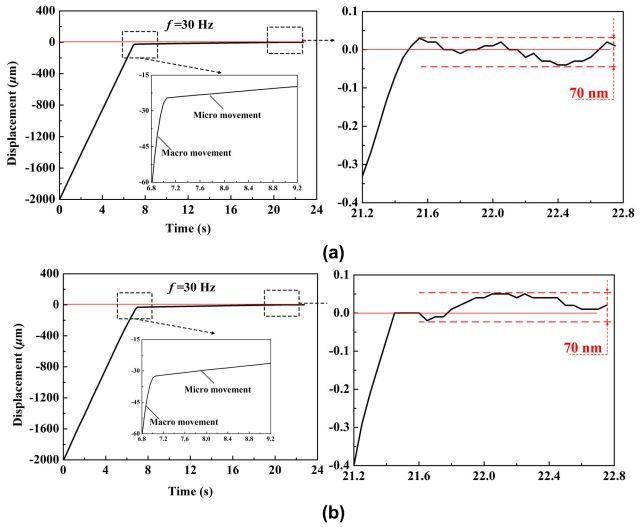

FIGURE 15. Positioning resolution of the proposed stage: (a) Freeload. (b) Load of 10 kg.

is shown in Fig. 14. At first, the target is set in the program on the computer. If the initial position of the prototype is far away from the target, the prototype will move to the target point with a fast speed and the driving voltage is V_1. When the prototype is close to the target, the prototype will move to the target point with a slow speed and the driving voltage is V_2. The V_1 is greater than V_2.

The driving frequency of 30 Hz is selected, because the ratio of backward motion is small and can move fast in macro movement. Fig. 15 (a) and Fig. 15 (b) show the positioning resolution of the prototype with free-load and with the load of 10 kg. It can be seen that the macro movement can effectively reduce the positioning time of the prototype from the experimental results. The micro movement is used to improve the positioning resolution. The initial position of the prototype is 2000 μm far away from the target. In macro movement, the driving voltage are both 100 V. In micro movement, the driving voltage are 4.0 V and 4.8 V when the prototype with free-load and the load of 10 kg. At last the positioning resolution of the prototype with free-load and with the load of 10 kg are both 70 nm.

V. CONCLUSION

In this paper, a piezoelectric stick-slip nanopositioning stage was proposed by introducing the load unit to make the driving unit separate from the moving unit, which improved the load capacity of the stage. The motion principle of the stage was illustrated and compared with the motion principle of the common stage. Additionally, a kinetic model was established and analyzed for the working process. A series of experiments were established to test the output characteristics of the stage. Experimental results confirm that the output performance of stage shows good linear relationships with the various driving voltages and frequencies in both directions. The velocities of the prototype are 4.75 mm/s and 4.86 mm/s in different directions under the sawtooth waveform of 100 V at 600 Hz. The resolution of the prototype is 30 nm and 33 nm in both directions. The proposed stage has a good performance in load capacity and driving capacity. When the load is 10 kg, the velocity of the stage is almost the same as that of free-load. In addition, the driving capacity of the prototype is more than 47.62 [(mm/s)g/mW].

REFERENCES

[1] S. Verma, W.-J. Kim, and H. Shakir, "Multi-axis maglev nanopositioner for precision manufacturing and manipulation applications," *IEEE Trans. Ind Appl.*, vol. 41, no. 5, pp. 1159–1167, Sep./Oct. 2005.
[2] S. Wang, H. Arellano-Santoyo, P. A. Combs, and J. W. Shaevitz, "Actin-like cytoskeleton filaments contribute to cell mechanics in bacteria," *Proc. Nat. Acad. Sci. USA*, vol. 107, no. 20, pp. 9182–9185, Oct. 2010.
[3] S.-T. Ho and S.-J. Jan, "A piezoelectric motor for precision positioning applications," *Precis. Eng.*, vol. 43, pp. 285–293, Jan. 2016.
[4] C. Chen, Y. Shi, J. Zhang, and J. Wang, "Novel linear piezoelectric motor for precision position stage," *Chin. J. Mech. Eng.*, vol. 29, no. 2, pp. 378–385, Mar. 2016.
[5] T. Tanikawa and T. Arai, "Development of a micro-manipulation system having a two-fingered micro-hand," *IEEE Trans. Robot. Autom.*, vol. 15, no. 1, pp. 152–162, Feb. 1999.
[6] Y. Zhang, K. K. Tan, and S. Huang, "Vision-servo system for automated cell injection," *IEEE Trans. Ind. Electron.*, vol. 56, no. 1, pp. 231–238, Jan. 2009.
[7] K. Uchino, "Piezoelectric actuator renaissance," *Phase Trans.*, vol. 88, no. 3, pp. 342–355, Jan. 2015.
[8] Z. M. Zhang, Q. An, J. W. Li, and W. J. Zahng, "Piezoelectric friction–inertia actuator—A critical review and future perspective," *Int. J. Adv. Manuf. Technol.*, vol. 62, nos. 5–8, pp. 669–685, Sep. 2012.
[9] H. Matthias, "Piezoelectric inertia motors—A critical review of history, concepts, design, applications, and perspectives," *Actuators*, vol. 6, no. 1, p. 7, Feb. 2017.
[10] T. Morita, "Miniature piezoelectric motors," *Sens. Actuators A, Phys.*, vol. 103, no. 3, pp. 291–300, Feb. 2003.
[11] K. Uchino, "Piezoelectric actuators: Expansion from IT/robotics to ecological/energy applications," *J. Jpn. Soc. Appl. Electromagn.*, vol. 20, no. 3, pp. 301–311, Aug. 2008.
[12] Y. Peng, Y. Peng, X. Gu, J. Wang, and H. Yu, "A review of long range piezoelectric motors using frequency leveraged method," *Sens. Actuators A, Phys.*, vol. 235, pp. 240–255, Nov. 2015.
[13] T.-W. Na, D.-H. Kang, J.-Y. Jung, J.-H. Han, and I.-J. Oh, "Linear-to-rotary motion converter using asymmetric compliant mechanics and single-crystal PMN-PT stack actuator," *J. Intell. Mater. Syst. Struct.*, vol. 25, no. 18, pp. 2221–2227, May 2014.
[14] Y. Tian, D. Zhang, and B. Shirinzadeh, "Dynamic modelling of a flexure-based mechanism for ultra-precision grinding operation," *Precis. Eng.*, vol. 35, no. 4, pp. 554–565, Oct. 2011.
[15] G.-Y. Gu, L.-M. Zhu, and C.-Y. Su, "High-precision control of piezoelectric nanopositioning stages using hysteresis compensator and disturbance observer," *Smart Mater. Struct.*, vol. 23, no. 10, Sep. 2014, Art. no. 105007.
[16] Y. Liu, W. Chen, J. Liu, and X. Yang, "A high-power linear ultrasonic motor using bending vibration transducer," *IEEE Trans. Ind. Electron.*, vol. 60, no. 11, pp. 5160–5166, Nov. 2013.
[17] Y. Liu, X. Yang, W. Chen, and D. Xu, "A bonded-type piezoelectric actuator using the first and second bending vibration modes," *IEEE Trans. Ind. Electron.*, vol. 63, no. 3, pp. 1676–1683, Mar. 2015.
[18] Y. Liu, W. Chen, X. Yang, and D. Xu, "A rotary piezoelectric actuator using the third and fourth bending vibration modes," *IEEE Trans. Ind. Electron.*, vol. 61, no. 8, pp. 4366–4373, Aug. 2014.
[19] T. Nishimura, H. H. Hosaka, and T. Morita, "Resonant-type smooth impact drive mechanism (SIDM) actuator using a bolt-clamped langevin transducer," *Ultrasonics*, vol. 52, no. 1, pp. 75–80, Jan. 2012.

[20] T. Yokose, H. Hosaka, R. Yoshida, and T. Morita, "Resonance frequency ratio control with an additional inductor for a miniaturized resonant-type SIDM actuator," *Sens. Actuators, A: Physical*, vol. 214, pp. 142–148, Aug. 2014.
[21] H. Huang, J. Li, H. Zhao, and C. Shi, "On the correlation between the structure and one stepping characteristic of a piezo-driven rotary actuator," *Microsyst. Technol.*, vol. 22, no. 12, pp. 2821–2827, Dec. 2016.
[22] T. Cheng, M. He, H. Li, X. Lu, H. Zhao, and H. Gao, "A novel trapezoid-type stick–slip piezoelectric linear actuator using right circular flexure hinge mechanism," *IEEE Trans. Ind. Electron.*, vol. 64, no. 7, pp. 5545–5552, Jul. 2017.
[23] Y. Li, H. Li, T. Cheng, X. Lu, H. Zhao, and P. Chen, "Note: Lever-type bidirectional stick-slip piezoelectric actuator with flexible hinge," *Rev. Sci. Instrum.*, vol. 89, no. 8, Aug. 2018, Art. no. 086101.
[24] Y. Zhang, Y. Peng, Z. Sun, and H. Yu, "A novel stick–slip piezoelectric actuator based on a triangular compliant driving mechanism," *IEEE Trans. Ind. Electron.*, vol. 66, no. 7, pp. 5374–5382, Jul. 2018.
[25] Q. Yao, J. Dong, and P. M. Ferreira, "Design, analysis, fabrication and testing of a parallel-kinematic micropositioning XY stage," *Int. J. Mach. Tools Manuf.*, vol. 47, no. 6, pp. 946–961, May 2007.
[26] L. Wang, J. Liu, S. Chen, K. Li, and Y. X. Liu, "Design and fabrication of a high-speed linear piezoelectric actuator with nanometer resolution using a cantilever transducer," *Smart Mater. Struct.*, vol. 28, no. 5, Apr. 2019. Art. no. 055035.
[27] L. Wang, Y. X. Liu, K. Liu, S. Chen, and X. Q. Tian, "Development of a resonant type piezoelectric stepping motor using longitudinal and bending hybrid bolt-clamped transducer," *Sens. Actuators A, Phys.*, vol. 285, pp. 182–189, Jan. 2019.
[28] H. Huang, H. Zhao, Z. Fan, H. Zhao, Z. Ma, and Z. Yang, "Analysis and experiments of a novel and compact 3-DOF precision positioning platform," *J. Mech. Sci. Technol.*, vol. 27, no. 11, pp. 3347–3356, Nov. 2013.
[29] J. Li, H. Huang, and H. Zhao, "A piezoelectric-driven linear actuator by means of coupling motion," *IEEE Trans. Ind. Electron.*, vol. 65, no. 3, pp. 2458–2466, Mar. 2018.
[30] Y. Wang, J. Zhu, M. Pang, J. Luo, S. Xie, M. Liu, L. Sun, C. Zhou, M. Tan, J. Ge, Y. Sun, and C. Ru, "A stick-slip positioning stage robust to load variations," *IEEE/ASME Trans. Mechatronics*, vol. 21, no. 4, pp. 2165–2173, Aug. 2016.
[31] S. Wang, W. Rong, L. Wang, Z. Pei, and L. Sun, "Design, analysis and experimental performance of a novel stick-slip type piezoelectric rotary actuator based on variable force couple driving," *Smart Mater. Struct.*, vol. 26, no. 5, Apr. 2017, Art. no. 055005.
[32] L. Wang, D. Chen, T. Cheng, P. He, X. Lu, and H. Zhao, "A friction regulation hybrid driving method for backward motion restraint of the smooth impact drive mechanism," *Smart Mater. Struct.*, vol. 25, no. 8, Jul. 2016, Art. no. 085033.
[33] T. Cheng, H. Li, M. He, H. Zhao, X. Lu, and H. Gao, "Investigation on driving characteristics of a piezoelectric stick–slip actuator based on resonant/off-resonant hybrid excitation," *Smart Mater. Struct.*, vol. 26, no. 3, Feb. 2017, Art. no. 035042.
[34] F. Qin, H. Huang, J. Wang, L. Y. Tian, T. W. Liang, and H. W. Zhao, "Design and stepping characteristics of novel stick–slip piezo-driven linear actuator," *Smart Mater. Struct.*, vol. 28, no. 7, Jun. 2019, Art. no. 075026.
[35] H. Li, Y. Li, T. Cheng, X. Lu, H. Zhao, and H. Gao, "A symmetrical hybrid driving waveform for a linear piezoelectric stick-slip actuator," *IEEE Access*, vol. 5, pp. 16885–16894, 2017.
[36] J. Wang, J. Li, Z. Xu, S. Wang, Z. Wang, B. Xu, Y. Sun, S. Liu, and H. Zhao, "Design, analysis, experiments and kinetic model of a high step efficiency piezoelectric actuator," *Mechatronics*, vol. 59, pp. 61–68, Mar. 2019.
[37] J. Wang, F. Qin, Y. Zhang, T. Liang, Z. Wang, B. Xu, Y. Sun, X. Liu, and H. Zhao, "Design, analysis and experiments of a linear piezoelectric actuator adopting a flexible mechanism with wing skeletal structure," *Smart Mater. Struct.*, vol. 28, no. 8, Jul. 2019, Art. no. 0085034.

YANG YU was born in Jilin, China, in 1995. He received the B.S. degree from the Changchun University of Technology, Changchun, China, in 2018, where he is currently pursuing the M.S. degree in mechanical engineering. His research interests include piezoelectric actuators and triboelectric nanogenerators.

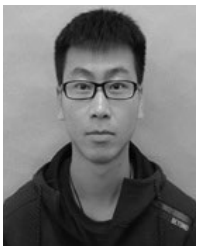

QIANG GAO was born in Shanxi, China, in 1994. He received the B.S. degree from the Luoyang Institute of Science and Technology, Luoyang, China, in 2018. He is currently pursuing the M.S. degree in mechanical engineering with the Changchun University of Technology. His research interests include friction drive mechanism and piezoelectric energy harvesting.

XIAOSONG ZHANG was born in Sichuan, China, in 1996. He received the B.S. degree from the Changchun University of Technology, Changchun, China, in 2019. His research interest includes piezoelectric actuators.

GUANGDA QIAO was born in Shandong, China, in 1997. He received the B.S. degree from the Changchun University of Technology, Changchun, China, in 2019, where he is currently pursuing the M.Eng. degree. His research interest includes piezoelectric actuators.

YI HAN was born in Jilin, China, in 1995. He received the B.S. degree from Jilin University, Changchun, China, in 2018. He is currently pursuing the master's degree in mechanical engineering with The University of Melbourne. His research interests include piezoelectric actuators.

XIAOHUI LU was born in Jilin, China. She received the B.S. degree in mathematics and applied mathematics from Beihua University, Jilin, in 2004, the M.S. degree in operational research and cybernetics from the Lanzhou University of Technology, Lanzhou, China, in 2007, and the Ph.D. degree in control theory and application from Jilin University, Changchun, China, in 2013. She was a Visiting Scholar with the School of College of Engineering, The Ohio State University, under the supervision of Junmin Wang, from 2017 to 2018. Her current research interests include vehicle powertrain control, model predictive control, data-driven control, and triboelectric nanogenerators.

TINGHAI CHENG received the B.S., M.S., and Ph.D. degrees from the Harbin Institute of Technology, in 2006, 2008, and 2013, respectively. He was a Visiting Scholar with the School of Materials Science and Engineering, Georgia Institute of Technology, from 2017 to 2018. He is currently a Professor with the School of Mechatronic Engineering, Changchun University of Technology. His research interests include piezoelectric actuators, piezoelectric energy harvester, and triboelectric nanogenerators.